

Temperature dependence of electronic structure on the ferroelectric phase transition of BaTiO₃


Yasuhisa Tezuka^{1,*}, Shunsuke Nozawa², Nobuo Nakajima³, and Toshiaki Iwazumi⁴

¹Graduate School of Science and Technology, Hirosaki University, 3 Bunkyo-cho, Hirosaki, Aomori 036-8561, Japan

²Photon Factory, Institute of Materials Structure Science, 1-1 Oho, Tsukuba, Ibaraki 305-0801, Japan

³Graduate School of Advanced Science and Engineering, Hiroshima University, 1-3-1 Kagamiyama, Higashi-Hiroshima, Hiroshima 739-8526, Japan

⁴Graduate School of Engineering, Osaka Prefecture University, Sakai, Osaka 599-8531, Japan

 (Received 23 March 2021; revised 15 September 2021; accepted 2 December 2021; published 23 December 2021)

X-ray Raman scattering spectra of ferroelectric BaTiO₃ were measured under excitation around the Ti *K*-absorption edge. Density of states of the unoccupied Ti *3d* state was measured using Ti *2p* core excitations. Anisotropy was observed in the ferroelectric phase with respect to spontaneous polarization direction. This anisotropy decreased with rising temperature and vanished in the paraelectric phase. Experimental results showed the ion displacement and electronic structure are closely related, and the hybridization between Ti *3d* and O *2p* states affects the ferroelectric phase transition.

DOI: [10.1103/PhysRevB.104.235148](https://doi.org/10.1103/PhysRevB.104.235148)

I. INTRODUCTION

Perovskite BaTiO₃ is one of the most important ferroelectric (FE) materials and the origin of its FE properties has long been a topic of discussion. The FE phase transition of perovskite materials is often classified as the displacive type [1,2]. However, several experimental [3–8] and theoretical studies [9,10] have suggested an anomalous behavior of the phase transition and a coexistence state of the order-disorder and displacive characters. The FE instability is affected by the hybridization between the Ti *3d* and O *2p* states [11]. Kuroiwa *et al.* reported the charge density distributions of PbTiO₃ and BaTiO₃, and demonstrated significant hybridization between Ti and O via the maximum-entropy method/Rietveld method [12]. To thoroughly understand the FE transition, the electronic structure of the Ti–O bond should be investigated further.

We recently reported the results of an x-ray Raman scattering (XRS) study of Ti oxides [13]. In that study, Ti *2p3d* core excitons, where the underlining denotes the core \bar{h} ole, were measured under excitations around the Ti *K*-absorption edge. The XRS spectra reflect the density of states (DOS) of the unoccupied Ti *3d* state. For insulator materials such as BaTiO₃, an inverse photoemission spectroscopy is ineffective for measuring the unoccupied DOS, just as a photoemission spectroscopy is ineffective for measuring the occupied DOS. Although x-ray absorption spectra/x-ray absorption fine structure (XAFS) can reflect the DOS of the unoccupied states, the core-hole potential strongly affects the spectra. An XRS measurement, which is a photon-in/photon-out method, will be suitable to investigate the electronic structure of insulator materials.

The azimuthal dependence of XRS results on BaTiO₃ has been previously reported [13]. The anisotropic electronic structure of the Ti *3d* state with respect to the *c* axis, which is the spontaneous polarization direction, was observed. In this study, the temperature dependence of XRS spectra was measured, as well as the detailed azimuthal dependence of the XRS. Temperature variation in the Ti *3d* state was closely related with the FE phase transition of BaTiO₃.

II. BACKGROUND

The scattering of light is described by the nonrelativistic interaction between an electron and the radiation. From the perturbation $\mathbf{p}\mathbf{A}$, where \mathbf{p} and \mathbf{A} are the momentum operator of the electron and the vector potential of the photon, respectively, the well-known Kramers-Heisenberg (KH) formula is derived [14–16]. The differential cross section of the photon scattering with respect to the solid angle Ω_{k_2} is expressed as [17]

$$\frac{d^2\sigma}{d\Omega_{k_2}d(\hbar\omega)} \sim \sum_j \left| \sum_i \frac{\langle j|T_2|i\rangle\langle i|T_1|g\rangle}{E_g + \hbar\Omega - E_i + i\Gamma_i} \right|^2 \times \delta(E_g + \hbar\Omega - E_j - \hbar\omega),$$

where $|g\rangle$, $|i\rangle$, and $|j\rangle$ are the initial, intermediate, and final states, respectively, and E_g , E_i and E_j are their respective energies, and $\hbar\Omega$ and $\hbar\omega$ are the photon energies and the operators T_1 and T_2 are the radiative transitions of the incident- and emitted-photons, respectively, and $\tau_i (= \hbar/\Gamma_i)$ is the lifetime of the intermediate state. The energy difference between the initial and the final states correspond to an elementary excitation in Raman process; phonon, magnon, electron excitations, etc. In this study, core level excitations were measured. Under the nonresonant condition, the formula corresponds to a Raman tensor determined by the symmetry of the elementary

*tezuka@hirosaki-u.ac.jp

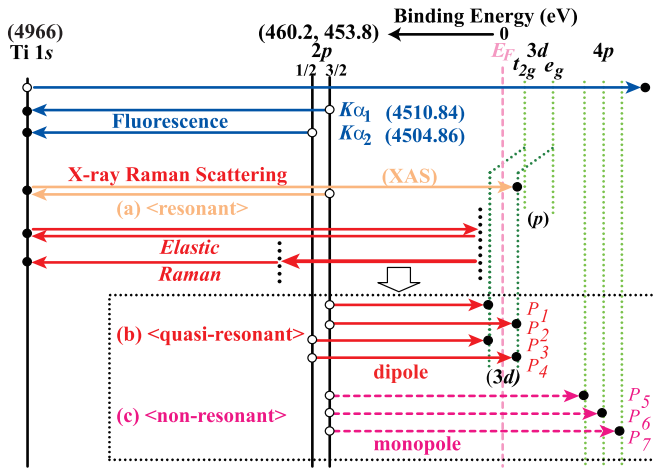


FIG. 1. Energy diagram of x-ray emission. The upper arrows represent the x-ray fluorescence process, while the lower arrows represent the x-ray Raman process. (a) Resonant XRS, (b) quasi-resonant XRS, and (c) normal (nonresonant) XRS. The full-length vertical dashed line denotes the Fermi level (E_F). The left side corresponds to the occupied state and the right side corresponds to the unoccupied state. The standard binding energies are shown in parentheses. The shorter vertical dashed lines in the XRS process denote virtual states.

excitation. Since the transition by a photon is a dipole transition, the excitations active in Raman scattering are monopole and quadrupole excitations, which changes orbital angular momentum ℓ with 0 and ± 2 , respectively. When the incident photon energy is close to the excitation threshold of the core electron, i.e., the resonant condition, some of the forbidden dipole excitation ($\Delta\ell = \pm 1$) selected by an intermediate state are enhanced and becomes observable. The Resonant XRS is often expressed as resonant inelastic x-ray scattering.

Figure 1 shows energy diagram of x-ray emission process in this experiment. The Fermi level (E_F) is indicated by the full-length vertical dashed line. The vertical solid lines on the left show the core levels, and the thin dotted lines on the right show the levels of the unoccupied states, which consist mainly of the Ti 3d and 4p states. The arrows on the top represent the Ti K fluorescence process. When the excitation energy is much higher than the binding energy of the Ti 1s core level, a core electron is emitted from the system, followed by an incoherent fluorescence process ($K\alpha_1$ and $K\alpha_2$). The lower part of Fig. 1 represents the XRS processes, which are coherent processes. Figure 1(a) shows the resonant XRS process. In the resonant process, the core electron is excited to an unoccupied state (conduction band) and another electron in an occupied state (valence band or core level) decays to the created core hole. The Ti 3d levels are shifted to a lower energy relative to the p levels, because of the core-hole potential [18], which is shown by the dotted lines. Figures 1(b) and 1(c) represent the XRS process described in this article. The excitation energy is lower than the absorption edge, so that the Ti 1s core electron is excited to a virtual state (represented by the dotted line to the left of E_F in Fig. 1). If the excited electron decays directly to the 1s core hole, the emitted photon undergoes elastic scattering.

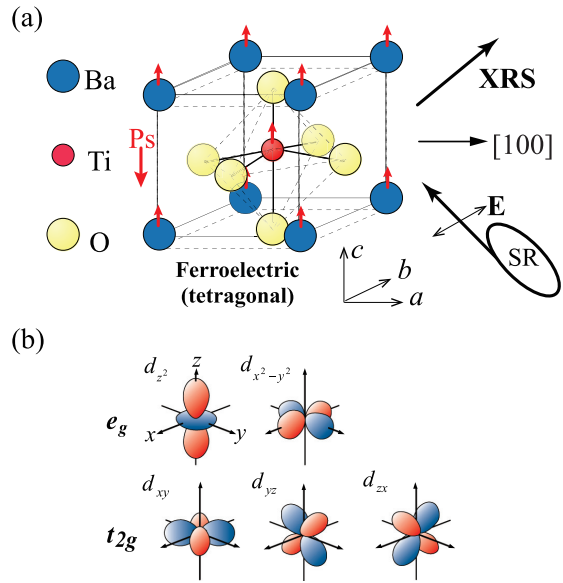


FIG. 2. (a) Crystal structure of ferroelectric BaTiO₃ and experimental configuration of XRS for the single crystal. The linearly polarized synchrotron radiation (SR) was irradiated on the (100) surface, and the vertically scattered XRS was measured. The sample was rotated around the [100] axis to measure the azimuthal dependence. (b) Shape of the 3d orbitals. These orbitals are split into t_{2g} and e_g symmetries by the crystal field in O_h symmetry.

If the excited system creates another elementary excitation such as Ti $\underline{2p}3d$ or Ti $\underline{2p}4p$ core excitation (represented in the dotted rectangle), where the underlining denotes the core hole, the excited state loses its energy and undergoes a transition to another virtual state (the dotted line to the left of the Ti 2p level in Fig. 1). The broad arrow in the middle of Fig. 1 denotes the energy transfer to the elementary excitation. As a result, the scattered photon has a lower energy than the excitation. When the excitation energy is sufficiently lower than that of the absorption edge, the normal (nonresonant) XRS process should be dominant, such that a monopole transition ($\underline{2p}4p$) would be active ($P_5 - P_7$). In the nonresonant XRS, such an even parity transition should be allowed [19]. Because the Ti $2p_{1/2}$ core hole decays rapidly by the Coster-Kronig process, only the Ti $\underline{2p}_{3/2}4p$ excitation would be observed.

III. EXPERIMENTAL

Figure 2(a) shows the unit cell of BaTiO₃ and the XRS experimental configuration. The XRS and Ti K XAFS experiments were performed at the bending magnet beamline BL7C of the Photon Factory, Institute of Materials Structure Science, KEK, Japan. These beamlines have focusing optics with a double-crystal monochromator. The XRS spectra were analyzed using an x-ray spectrometer [20]. Synchrotron radiation (SR) under linear-polarization in a horizontal plane was irradiated, and the vertically scattered x-rays were analyzed using a Ge(400) crystal. Furthermore, the emission spectra exhibiting energy around the Ti K α fluorescence lines ($K\alpha_1 = 4510.84$ eV and $K\alpha_2 = 4504.86$ eV) [21] were measured. The analyzed x-rays were detected through a position-sensitive proportional counter using the charge-division method. The

energy resolution for the Ti K XAFS and XRS measurements was approximately 1 eV for a 5-keV photon. The measurements were performed in vacuum (approximately 10^{-3} Pa). Because XRS is photon-in/photon-out measurements, bulk properties of the sample can be measured. The XAFS spectra of the powdered sample were measured via the transmission method at RT. The partial photon yield (PPY) method was used to measure the absorption spectra for single crystals. The PPY measures the numbers of fluorescence and scattering photons in the energy range of XRS measurement, i.e., total photon numbers in a XRS spectrum, with changing excitation energy. Though this method is often called as partial fluorescence yield (PFY), the notation PPY is used in this article.

The temperature dependences of XAFS and XRS were also measured. BaTiO₃ undergoes an FE phase transition from the tetragonal (C_{4v}) FE phase to a cubic (O_h) paraelectric (PE) phase at about 120°C. Because the phase transition is of the first order, measurements should be performed under warming process. A sample holder with a heater was rotated along the [100] axis to measure the azimuthal dependence at each temperature. For the given XRS measurement conditions, the temperature of the sample holder was monitored; this temperature was slightly different from the sample temperature. Figure 2(b) shows the orbital shapes of Ti $3d$ states. The unoccupied Ti $3d$ state was split into t_{2g} and e_g states by the crystal field in an O_h symmetry. Although BaTiO₃ is slightly distorted and exhibits a tetragonal symmetry (C_{4v}) at RT, the notations of t_{2g} and e_g will be used herein.

Detailed azimuthal dependent XRS in FE phase was measured using piezo-driven rotator (attocube systems AG, Germany) in vacuum, which was controlled from outside the measurement chamber. The azimuth angle of sample was changed 5° at a time around [100] axis.

Commercially obtained powder (Furuuchi Chemical Co., Japan) and single domain crystals of BaTiO₃(100) (Neutron Co., Japan) were used herein. Resonant XRS spectra and the azimuthal dependence of the XRS spectra were measured using single crystals. BaTiO₃ has a perovskite structure. Cations (Ti⁴⁺ and Ba²⁺ having nominal ionic valence) were displaced along the c axis relative to the anion (O²⁻) site and exhibited FE properties, as shown in Fig. 2(a). Owing to the ion displacement, spontaneous polarization (\mathbf{P}_S) is produced along the c axis. Note that the distance between Ti and O considerably changes along the c axis, whereas the changes along the ab plane are minor.

IV. RESULTS AND DISCUSSIONS

A. Resonant x-ray Raman scattering

Figure 3 shows x-ray absorption spectra of BaTiO₃ at the Ti K -absorption edge, which were measured at RT (FE phase). Figure 3(a) shows XAFS spectrum of powder sample. Figure 3(b) shows azimuthal dependent PPY spectra of single crystal BaTiO₃(100). The lines and circles show the spectra measured under the excitation of E// c and E// b , respectively. The main structure above 4978 eV reflects unoccupied Ti $4p$ state, while pre-edge region under 4978 eV reflects unoccupied Ti $3d$ state. The PPY spectra show an obvious azimuthal dependence. On the basis of the calculations using the full multiple scattering method, Vedrinskii *et al.* suggested that the

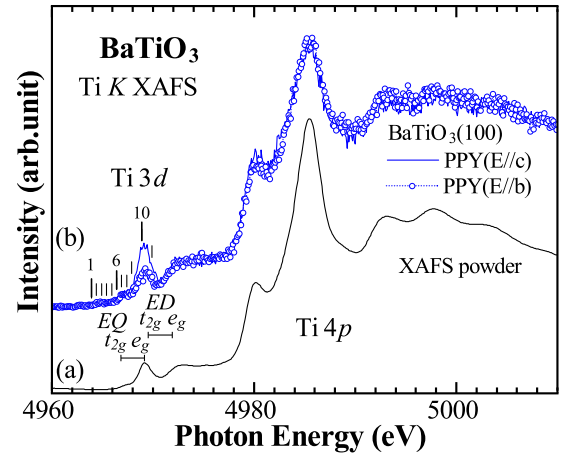


FIG. 3. X-ray absorption spectra of BaTiO₃. (a) XAFS of powder. (b) PPY of BaTiO₃(100) (Line: E// c , Circle: E// b). Vertical bars and numbers denote excitation energy in resonant XRS study.

peak intensity is strongly related to the displacement of the Ti ion [22]. On the other hand, according to Uozumi *et al.*, the pre-edge structure comprises an electric dipole (ED) and electric quadrupole (EQ) transition, both of which are split into t_{2g} and e_g by the crystal field [18]. These structures overlap, as shown in Fig. 3, and three structures are observed in the pre-edge region. The peak at approximately 4968 eV showing a remarkable azimuthal dependence may be considered to possess both ED and EQ components; thus, the temperature dependence of the peak is not easily comprehensible. Vertical bars and numbers in Fig. 3 denote excitation energy in resonant XRS study.

Figure 4 shows polarization dependent resonant x-ray emission spectra (XES) of BaTiO₃(100). X-ray emission spectra around Ti $K\alpha$ fluorescence were measured under excitation at pre-edge region of Ti K absorption. Numbers at right side of spectra denote excitation energies shown in Fig. 3. The lines and circles show the spectra measured under the excitation of E// c and E// b , respectively. Each spectrum was plotted after magnification by the factor at left side. Fluorescence like spectra was observed at high energy excitation (#11). The x-ray emission spectra become weak and shift to lower energy with lowered excitation energy, and then shows many structures.

Figure 5 shows polarization dependent resonant x-ray Raman scattering spectra of BaTiO₃(100). The x-ray emission spectra in Fig. 4 are plotted against the energy loss (Raman shift) from the excitation energy. The lines and circles show the spectra under the excitation E// c and E// b , respectively. The spectra show seven structures independent from excitation energy, suggesting there are seven elementary excitations in XRS spectra. P₁-P₄ correspond to the Ti $3d$ state, whereas P₅-P₇ correspond to the Ti $4p$ state [13]. The $3d$ state is split into four peaks through the spin-orbit splitting of the Ti $2p$ state and the crystal field splitting of the Ti $3d$ state. Owing to the selection rules of XRS, a monopole transition such as $2p4p$ is active under the nonresonant condition and a dipole transition such as $2p3d$ is prohibited under this nonresonant condition. However, the dipole transition is enhanced under resonance and becomes observable [13]. Peaks P₁-P₄ are

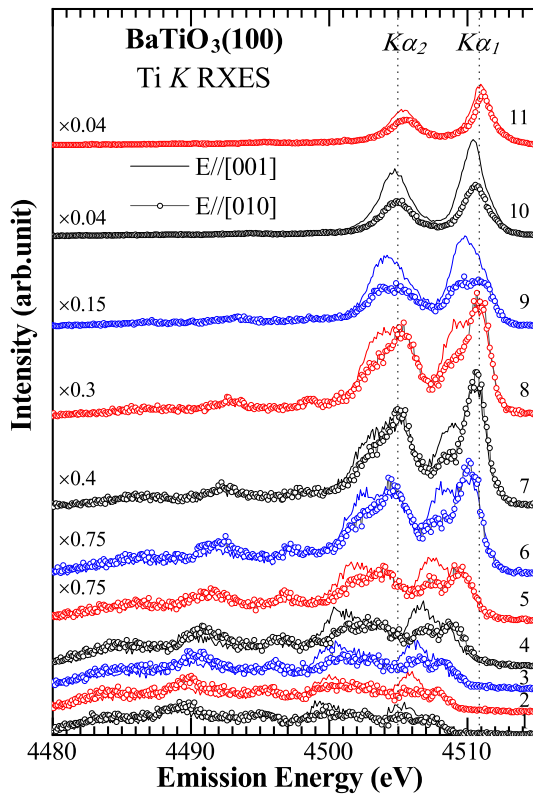


FIG. 4. Polarized dependent Ti K resonant x-ray emission spectra of $\text{BaTiO}_3(100)$. Line: $E//c$, Circle: $E//b$. Numbers at right denote excitation energy shown in Fig. 3. Each spectrum was plotted after magnification by the factor at left. Vertical dot lines denote Ti $K\alpha$ fluorescence energies. Vertical dotted lines show Ti $K\alpha$ fluorescence energies.

enhanced under the $3d$ resonance, whereas peaks P_5 – P_7 are unaffected by the excitation energy. Although the resonance effect of each t_{2g} and e_g peak is strong under excitation at the corresponding peak energy of XAFS, each peak becomes single peak as shown in Fig. 5 (#10); hence, the peak intensities cannot be compared. Thus, in the azimuthal and temperature dependence experiments, the excitation energy below the pre-edge peak is selected, so that t_{2g} and e_g peaks in the XRS spectrum have comparable intensities. Furthermore, the XRS reflects the unoccupied partial DOS's of not only the $3d$ state but also the $4p$ state, whereas the XAFS includes the extended x-ray absorption fine structure (EXAFS) component at a high energy, and hence, the x-ray absorption and EXAFS components are mixed. The XRS measurement has the advantage that it can separate each state in one spectrum, allowing a comparison of these states.

B. Azimuthal dependence

Figure 6 shows azimuthal dependent XRS spectra of $\text{BaTiO}_3(100)$ measured at RT. The energy-dependent XRS of $\text{BaTiO}_3(100)$ with an azimuthal dependence has been reported [13]. In this experiment, detailed azimuthal dependence was measured. The polarization of excitation photon in XRS was changed by rotating 5° at a step around the [100] axis from $E//c$ (0°) to $E//b$ (90°), and then $E//b$ (90°) to $E//c$ (180°). The excitation energy of XRS was 4965.5 eV (#6

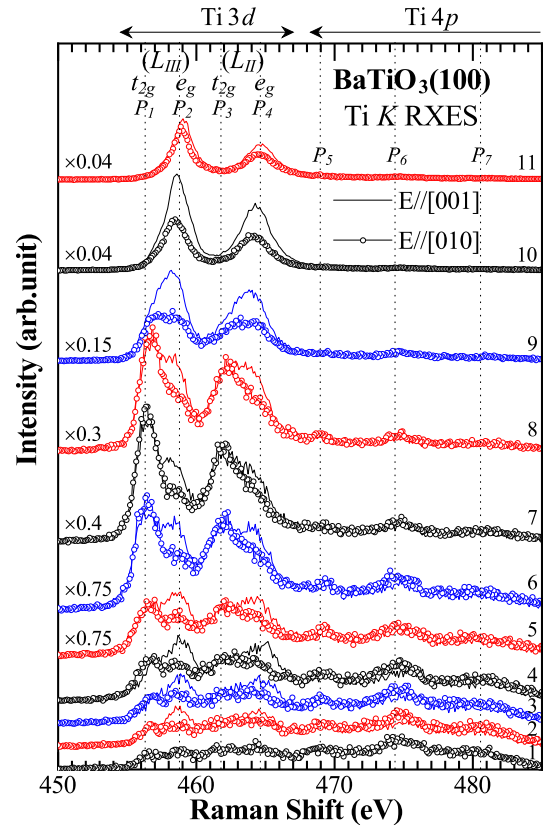


FIG. 5. Polarized dependent Ti K resonant x-ray Raman scattering spectra of $\text{BaTiO}_3(100)$. The XES spectra were plotted against energy loss from excitation energy (Raman Shift). Line: $E//c$, Circle: $E//b$. Numbers at right denote excitation energy shown in Fig. 3. Each spectrum was plotted after magnification by the factor at left. Vertical dotted lines denote Raman peaks.

in Fig. 3), so that the intensities of t_{2g} and e_g peaks in XRS are comparable. The lower panel shows azimuthal dependent XRS spectra and the upper panel shows its intensity mapping.

The Ti $3d$ peaks (P_1 – P_4) show remarkable azimuthal dependence, while Ti $4p$ peaks (P_5 , P_6) do not show azimuthal dependence. The t_{2g} peaks show almost fourfold symmetry, while the e_g peaks show twofold symmetry. The orbit of t_{2g} state is directed between ligand O ions, thus the t_{2g} state has nearly fourfold symmetry even in tetragonal phase. In the case of e_g state, the orbit is directed to ligand O ion that is displaced along the c axis, thus the e_g state has twofold symmetry in (100) plane. The result that the intensity of e_g peaks in XRS that reflects unoccupied DOS decreases along the c axis means increased $3d$ electron in e_g state, that is, increased hybridization between Ti and O.

C. Temperature dependence

Figure 7 shows the x-ray absorption spectra of BaTiO_3 at the Ti K -absorption edge. The inset shows the whole XAFS spectra of the powder sample measured using the transmission method at RT. The top of the main panel Fig. 7(a) shows the pre-edge region of the XAFS. Figures 7(b)–7(d) shows the PPY spectra of $\text{BaTiO}_3(100)$ at 150°C (PE), 120°C ($\sim T_C$), and RT (FE), respectively. The lines and circles show the spectra measured under the excitation of $E//c$ and $E//b$,

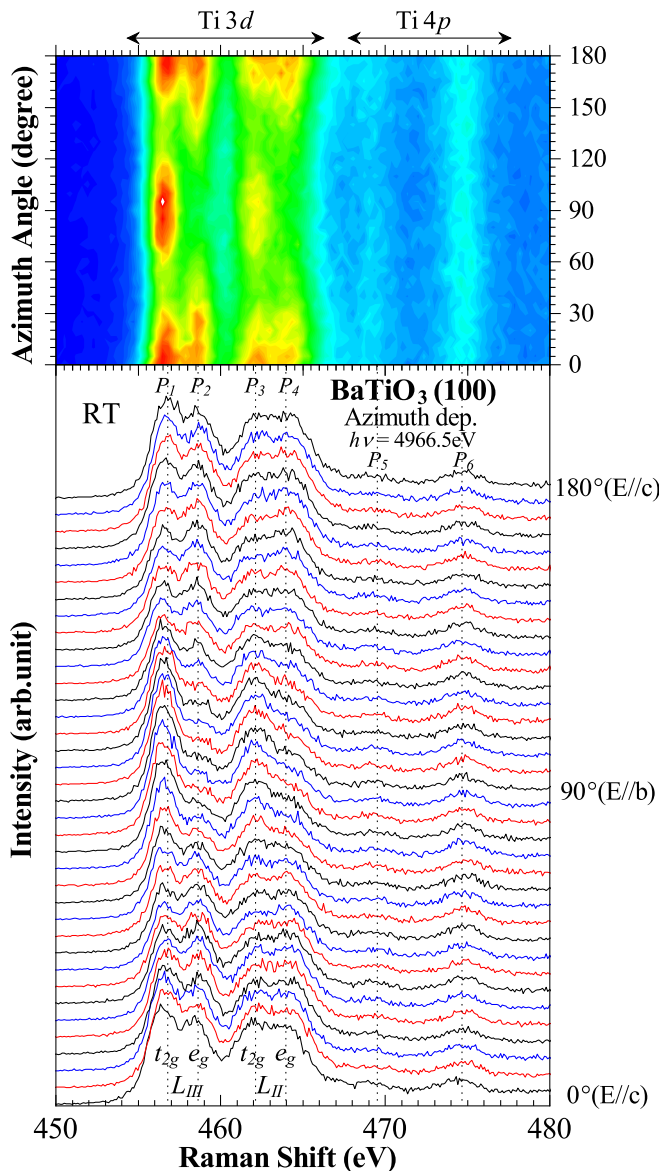


FIG. 6. Azimuthal dependent x-ray Raman scattering spectra of $\text{BaTiO}_3(100)$. Excitation energy was 4966.5 eV. Azimuth angle was changed by rotating 5° at a step around $[100]$ axis. Polarization of incident photon was changed from $E//c$ to $E//b$, then $E//b$ to $E//c$.

respectively. The PPY spectra show an obvious azimuthal dependence in the FE phase and then show no distinct difference in the PE phase.

Figure 8 shows the temperature-dependent XRS of $\text{BaTiO}_3(100)$ excited at 4965.5 eV (#6 in Fig. 3) in two polarization configurations. The XRS spectra were measured at several temperatures under both polarizations. The measurements were performed under warming process from RT (FE phase) to high temperature (PE phase). The polarization of XRS was changed by rotating sample in every temperature.

The $3d(e_g)$ states (P_2 , P_4) exhibit strong azimuthal and temperature dependences, whereas the $3d(t_{2g})$ states (P_1 , P_3) do not show an azimuthal dependence, and the $4p$ states (P_5 – P_7) remain unchanged. The temperature dependence of the anisotropy of the Ti $3d$ state can be verified. The anisotropy in the FE phase decreases with the rising

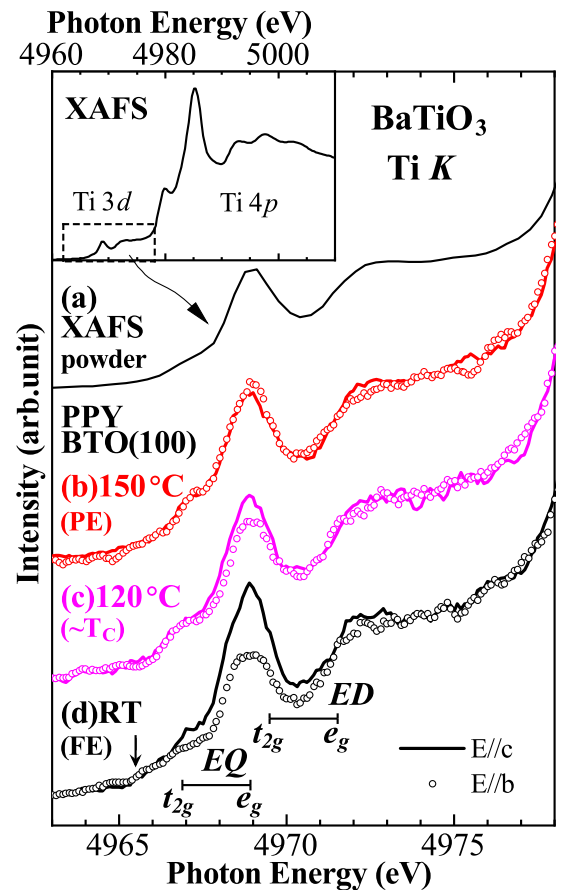


FIG. 7. Temperature-dependent absorption spectra at the Ti K -absorption edge. Inset shows the whole XAFS of powder BaTiO_3 at RT and top of main panel (a) shows the pre-edge region of XAFS. Lower parts show the PPY spectra of $\text{BaTiO}_3(100)$. (b) 150°C , (c) 120°C , (d) RT. Lines and circles show the spectra under the excitation of $E//c$ and $E//b$, respectively. The arrow shows the excitation energy of XRS measurements.

temperature and seems to vanish in the PE phase within the experimental errors. As the XRS spectrum reflects an unoccupied state, the decrease in peak intensity suggests the increase in the number of Ti $3d$ electrons. The results suggest that the bonding along the c axis is strong in the FE phase but it weakens with rising temperature and it becomes almost identical with the other axes in the PE phase.

Figure 9 shows the temperature dependence of the asymmetry of the Ti $3d$ peak. The square of asymmetry index $A = (I_b - I_c)/(I_b + I_c)$ of each peak was plotted against temperature. P_2 shows a linear relation on $\Delta T = T_C - T$, as denoted by the dotted straight line, and P_4 shows a nearly linear dependence, whereas P_1 and P_3 do not change with temperature. Because P_4 originates from the excitation in the $2p_{1/2}$ core state, the XRS can be affected by the core-hole potential and many body effects, such as the Coster-Kronig effect [23]. The temperature dependence may also be affected by another structural phase transition to the orthorhombic phase (C_{2v}) of BaTiO_3 at approximately $T \sim 5^\circ\text{C}$. The differences in the XRS intensity reflect the anisotropy of the Ti–O bond, and this anisotropy can be explained by the displacement between the anion (O) and cation (Ti).

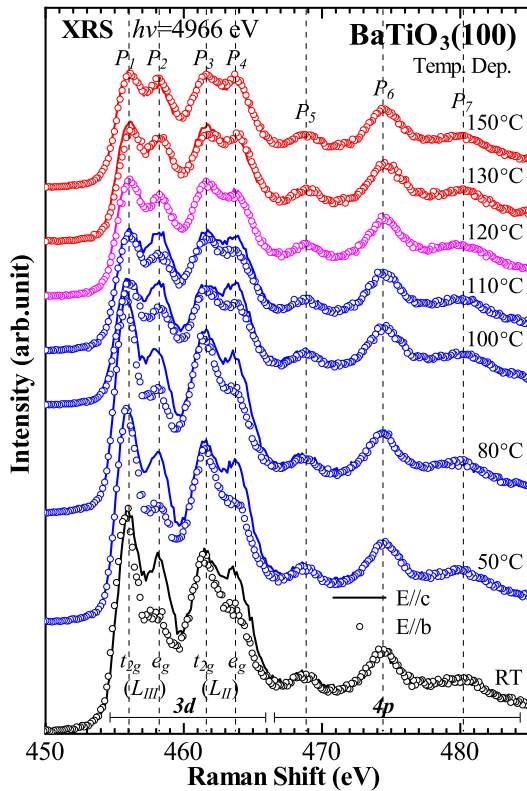


FIG. 8. Temperature-dependent XRS spectra of BaTiO₃(100). Excitation energy is 4965.5 eV at the pre-edge of XAFS. Temperatures are shown beside the spectra. The lines and circles show the spectra under the excitation of E//c and E//b, respectively.

Before performing this XRS experiment, temperature dependence measurements under E//c and E//b configurations were independently performed for different time periods and samples. In this experiment, these results were confirmed through the measurements performed on a sample by rotating the sample. Because XRS measurements are time consuming, few data points were obtained in this experiment. However, the reproducibility of data was confirmed through several experiments.

The results resemble the temperature dependence of spontaneous polarization (P_s) [24] as shown in Fig. 9, however, no abrupt jumps were observed at the transition temperature in this experiment. Furthermore, the change appeared to be a second-order transition [25,26]. Note that these results reflect only the Ti 3d state and not the Ba state. Though the contribution of the Ba atom at the corner site is indispensable for the FE properties and we cannot discuss the type of the phase transition, it is clear that the Ti 3d state is crucial in the phase transition. Other XRS measurements show that a charge transfer excitation between the O 2p and Ti 3d states changes the energy in the FE phase transition [27]. This result is considered to be very closely related with the hybridization change herein. The XRS results will be useful in understanding these phase transitions.

Although it has been previously reported that hybridization affects FE phase transitions, the results obtained herein are the first clear evidence of the relation between the electronic state

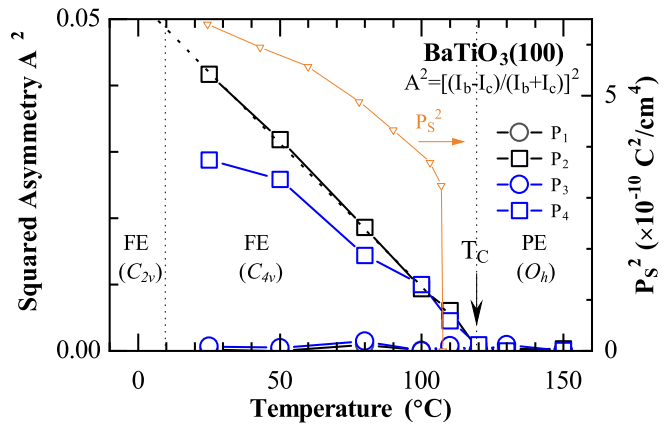


FIG. 9. Temperature dependence of peak asymmetry between the spectra under the excitation of E//c and E//b. The square of asymmetry A^2 of each 3d peak was plotted. The dotted line shows the straight line proportional to $(T_C - T)$, where T_C is the ferroelectric phase transition temperature. Triangles show squared spontaneous polarization (P_s) [24].

and FE phase transition. Furthermore, a theoretical examination could provide new information.

Herein, the beam spot size of the excitation SR was approximately 1 mm². Hence, the results reflect the macroscopic state of BaTiO₃. It was suggested that the disordered microdomain is crucial in the PE phase [7,28], but such a microdomain could not be detected in this study. Thus, we cannot draw a conclusion about the ferroelectric transition mechanism of BaTiO₃. Using a microfocus beam for XRS measurements may enable detection of such microdomains.

V. CONCLUSION

The resonant x-ray Raman scattering of BaTiO₃ was measured at the Ti *K*-absorption edge. The core excitations of $2p3d$ and $2p4p$ were measured. The spectra reflect the unoccupied state of the Ti 3d and 4p states. The 3d(e_g) state is anisotropic in the FE phase and becomes degenerate in the PE phase, whereas the 4p state remains unchanged. These results indicate the anisotropy of the Ti–O bond in the FE phase and the degeneracy in the PE phase. The changes in the temperature are very closely related with the FE phase transition. These results prove that the Ti–O covalency is crucial in FE phase transitions.

The XRS measurements offer information about the electronic state of the bulk state even in insulator materials and will be a powerful technique for conducting research on the electronic states.

ACKNOWLEDGMENTS

The authors thank Professor Isozumi for the use of his detector and the staff of the Photon Factory for their assistance with machine operations. This work has been performed with the approval of the Photon Factory Program Advisory Committee (Proposals No. 2004G193, No. 2006G232, No. 2008G682, and No. 2010G697). We thank the Edanz Group [29] for editing a draft of this manuscript.

- [1] W. Cochran, *Adv. Phys.* **9**, 387 (1960); **10**, 401 (1961).
- [2] J. Harada, J. D. Axe, and G. Shirane, *Phys. Rev. B* **4**, 155 (1971).
- [3] R. Comes, M. Lambert, and A. Guinier, *Solid State Commun.* **6**, 715 (1968).
- [4] Y. Luspín, J. L. Servion, and F. Gervais, *J. Phys. C* **13**, 3761 (1971).
- [5] H. Vogt, J. A. Sanjurjo, and G. Rossbroich, *Phys. Rev. B* **26**, 5904 (1982).
- [6] K. Inoue, *Ferroelectrics* **52**, 253 (1983).
- [7] B. Ravel, E. A. Stern, R. I. Vedrinskii, and V. Kraizman, *Ferroelectrics* **206**, 407 (1998).
- [8] B. Zalar, V. V. Laguta, and R. Blinc, *Phys. Rev. Lett.* **90**, 037601 (2003).
- [9] M. Stachiotti, A. Dobry, R. Migoni, and A. Busmann-Holder, *Phys. Rev. B* **47**, 2473 (1993).
- [10] H. Takahasi, *J. Phys. Soc. Jpn.* **16**, 1685 (1961).
- [11] R. E. Cohen, *Nature (London)* **358**, 136 (1992).
- [12] Y. Kuroiwa, S. Aoyagi, A. Sawada, J. Harada, E. Nishibori, M. Takata, and M. Sakata, *Phys. Rev. Lett.* **87**, 217601 (2001).
- [13] Y. Tezuka, T. Sasaki, Y. Fujita, T. Iwamoto, H. Osawa, S. Nozawa, N. Nakajima, H. Sato, and T. Iwazumi, *J. Phys. Soc. Jpn.* **83**, 014707 (2014).
- [14] W. Heitler, in *The Quantum Theory of Radiation*, 3rd ed. (Dover, New York, 1984), p. 190.
- [15] W. Schülke, in *Electron Dynamics by Inelastic X-Ray Scattering* (Oxford Science, Oxford, 2007), p. 7.
- [16] J. J. Sakurai, in *Advanced Quantum Mechanics* (Addison-Wesley, London, 1967), p. 49.
- [17] A. Kotani and S. Shin, *Rev. Mod. Phys.* **73**, 203 (2001); F. M. F. de Groot and A. Kotani, in *Core Level Spectroscopy of Solid* (CRC Press, Boca Raton, FL, 2008), p. 339.
- [18] T. Uozumi, K. Okada, A. Kotani, O. Durmeyer, J. P. Kappler, E. Beaupaire, and J. C. Parlebas, *Europhys. Lett.* **18**, 85 (1992).
- [19] For example: W. Hays and R. Roudon, in *Scattering of Light by Crystal* (Dover, New York, 1978), p. 48.
- [20] T. Nakamura, H. Shoji, S. Nanao, T. Iwazumi, S. Kishimoto, R. Katano, and Y. Isozumi, *Phys. Rev. B* **62**, 5301 (2000).
- [21] *X-Ray Data Booklet*, edited by A. Thompson and D. Vaughan (Lawrence Berkeley National Laboratory, Berkeley, CA, 2001).
- [22] R. V. Vedrinskii, V. L. Kraizman, A. A. Novakovich, Ph. V. Demekhin, and S. V. Urazhdin, *J. Phys.: Condens. Matter* **10**, 9561 (1998).
- [23] D. Coster and R. Kronig, *Physica* **2**, 13 (1935).
- [24] W. J. Merz, *Phys. Rev.* **76**, 1221 (1949); **91**, 513 (1953).
- [25] For example: C. Kittel, in *Introduction to Solid State Physics*, 8th ed. (Wiley, New Jersey, 2005), p. 475.
- [26] K. Deguchi and E. Nakamura, *Phys. Rev. B* **5**, 1072 (1972).
- [27] Y. Isohama, N. Nakajima, H. Maruyama, Y. Tezuka, and T. Iwazumi, *J. Elec. Spec. Relate. Phenom.* **184**, 207 (2011).
- [28] L. A. Bursill and P. Lin, *Nature (London)* **311**, 550 (1984).
- [29] <https://en-author-services.edanz.com/ac>